Photonic generation of millimeter and terahertz waves with high phase stability

Dongning Sun, Yi Dong,* Lilin Yi, Siwei Wang, Hongxiao Shi, Zongyang Xia, Weilin Xie, and Weisheng Hu

State Key Laboratory of Advanced Optical Communication Systems and Networks, Shanghai Jiao Tong University, 800 Dong Chuan Road, Shanghai 200240, China

**Corresponding author: yidong@sjtu.edu.cn*

Received December 5, 2013; accepted January 30, 2014;
posted February 11, 2014 (Doc. ID 202592); published March 11, 2014

Optical generation of highly stable millimeter and terahertz waves is proposed and experimentally demonstrated. The optical-fiber-path-induced phase fluctuation is identically transferred to a 40 MHz intermediate frequency by using dual-heterodyne phase error transfer, then canceled by a phase-locked loop. Based on the scheme, highly stable signals within the frequency range from 25 GHz to 1 THz are generated, and the phase jitter is decreased from 2.05 rad to 4.7 mrad in the frequency range from 0.01 Hz to 1 MHz. For 1 THz, the residual phase noise reaches −60 dBc/Hz at 1 Hz frequency offset from the carrier, and the relative timing jitter is reduced to 0.7 fs. © 2014 Optical Society of America

OCIS codes: (060.5625) Radio frequency photonics; (120.5050) Phase measurement; (070.1170) Analog optical signal processing.

http://dx.doi.org/10.1364/OL.39.001493

The millimeter-wave (mm-wave) region of the electromagnetic spectrum, also called the extremely high frequency region, corresponds to radio frequencies from 30 to 300 GHz. The signals in this frequency band are widely used in many areas such as wireless access networks [1,2], radio-over-fiber systems [3], and phase-array millimeter-wave antennas [4]. In addition, the frequency range from 300 GHz to terahertz has been widely utilized in astronomic applications such as in the atacama large millimeter array (ALMA) [5] and the Herschel Space Observatory (Herschel) [6]. Moreover, molecules can be distinguished from others by their own THz fingerprints which enable various practical applications such as analytical science, global environmental monitoring, and security [7–10]. In most cases, phase stability and spectral purity of the source determine the main properties of the system such as sensitivity, range, capacity, and bandwidth. For example, in spectroscopic measurement areas, high phase stability reduces absolute frequency errors and false alarms [11–13]. Therefore, a single source that can cover both mm and THz waves with high phase stability is highly desired for fulfilling such versatile applications. Unfortunately, conventional electronic approaches suffer from limited frequency and bandwidth, high conducting losses, and susceptibility to electromagnetic interference (EMI).

Photonic mm/THz wave generation systems are very attractive due to their wide bandwidth, light weight, and anti-EMI characteristics [14,15]. Recently, a remarkable work using the modulation-sideband-injection locking method to generate tunable signals from 0.5 to 110 GHz has been reported [16] which shows the powerful capacity of photonic radio frequency systems. Among a number of photonic techniques generating mm waves proposed so far, employing heterodyning of two phase-locked optical carriers derived from a highly coherent optical frequency comb (OFC) has been considered as a good choice due to its very wide spectral coverage up to terahertz and low phase noise [17–21]. Three common methods of obtaining two optical carriers are optical phase-locking of two lasers to two lines of an OFC, filtering out two lines from an OFC with an optical filter, or injection-locking two lasers to two lines of an OFC. The first method concerning the optical phase-locked loop (OPLL) has a rigorous requirement of laser linewidth and a complex configuration. The latter two methods feature a simple configuration and a lower requirement of laser linewidth. However, the two optical carriers' phases fluctuate due to temperature variation and mechanical perturbation along the two separate optical fiber paths, which severely degrades the phase stability of generated mm/THz signals. Therefore, it is necessary to detect and cancel the optical-path-induced phase fluctuations to improve the signal phase stability. But it is difficult to detect the phase fluctuation in the mm/THz waves region using conventional approaches and few works have been reported to solve this significant issue.

In this Letter, we describe a highly stable mm/THz wave generation system based on the dual-heterodyne phase error transfer (DHPT) scheme and a coherent OFC generator. In our system, phase noise induced by a separate optic path is detected using DHPT and canceled with an acousto-optic frequency shifter (AOFS) which is used to correct the mm/THz phase. Compared to the OPLL-based methods, lower requirements are imposed on the linewidth of the laser used, thus reducing system complexity.

The basic scheme of DHPT is described as follows. In order to detect the phase fluctuation of the generated mm/THz wave signal, which is determined by the phase difference of two optical carriers, two separate lines of OFC are frequency-shifted by different intermediate frequencies (IF), then heterodyned with the original OFC, obtaining two intermediate-frequency signals (IF1 and IF2) at a low-bandwidth photodetector (PD). Then the phase difference of IF1 and IF2 is transferred to a new beating signal (IF3) by low-frequency electrical heterodyne beating for phase detection. In this case, the phase fluctuation of the generated mm/THz wave is transferred to IF3. The detected phase error is fed to a phase-locked-loop (PLL) controlled AOFS that is

employed to adjust phase difference of the two optical carriers and thus the phase of generated mm/THz signals. Finally, the phase fluctuation is canceled by the PLL-controlled AOFS and a highly stable mm/THz wave is obtained. Therefore, the DHPT permits low-frequency components in MHz region to detect mm/THz wave phase information while it is independent of the frequency of the desired mm/THz wave, which significantly reduces the difficulty of detecting the phase of the mm/THz wave. By employing this scheme, the phase noise performance of generated signals is improved by about 30 dB at 1 Hz frequency offset from the carrier compared with the open loop case for the frequencies of 25 GHz, 50 GHz, 100 GHz, 500 GHz, and 1 THz. For all the above generated mm/THz waves, the phase noises are kept under −28 dBc/Hz, −58 dBc/Hz, and −80 dBc/Hz at 0.01, 1, and 100 Hz frequency offset from the carrier, respectively.

The experimental setup of the proposed scheme is shown in Fig. 1. A laser operating at 1550 nm with less than 3 kHz linewidth is fed as a seed into an optical frequency comb generator (OFCG) based on a Fabry–Perot electro-optic modulator with 2.5 GHz free spectral range (FSR). The OFCG is driven by a low phase noise microwave synthesizer (Anritsu model MG3694B) at 25 GHz, which produces an OFC with a 25 GHz frequency interval and more than a 10 THz spectral span. It is feasible to generate about a 1 THz signal in this system according to the 7 dB/THz power decreasing characteristic of the OFCG. The output from OFCG is split into two branches by a polarization-maintaining fiber coupler (PMC1). One branch is used as reference and the other one is frequency up-shifted with 35 MHz by AOFS1. Then the nth and mth lines of OFC are separated into optical fiber path "a" and "b," respectively, by an arrayed waveguide grating (AWG) with 25 GHz spacing which is used to select two arbitrary lines of the OFC. AOFS2 on path "b" driven by a 40 MHz voltage-controlled crystal oscillator (VCXO) is used as part of the phase-locked loop to compensate the optical-path-induced phase fluctuations. A 10 MHz rubidium oscillator is used as the frequency standard. Both the 25 GHz microwave synthesizer and the 35 MHz AOFS1-driven signal are synchronized with this rubidium oscillator.

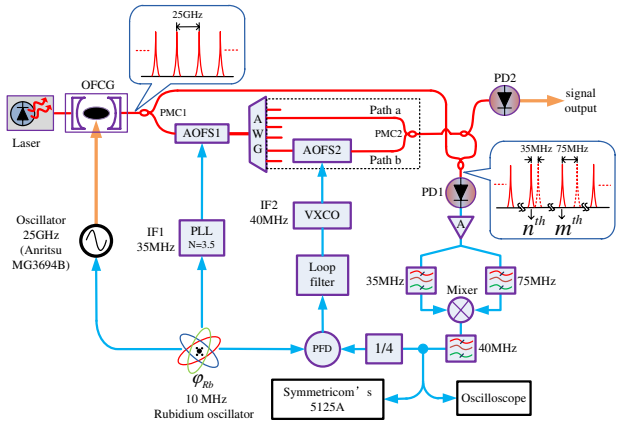

Fig. 1. Experimental setup for the high phase stability mm/THz wave generation system based on DHPT. Insets: illustrative output optical spectrum of OFCG and the mm/THz wave phase detector frequency diagram. OFCG, optical frequency comb generator; PMC, polarization-maintaining coupler; AOFS, acousto-optic frequency-shifter; AWG, arrayed waveguide grating; PLL, phase-locked loop; IF, intermediate frequency; VCXO, voltage-controlled crystal oscillator; PFD, digital phase and frequency detector; PD, photo-detector; A, amplifier.

The selected two lines from the OFC can be written as

$$E_n(t) = \exp\{j[(\omega_s + n\omega_{\mathrm{RF}} + \omega_{35M})(t + \tau_a(t)) + \varphi_n + \varphi_{35M}]\}, \tag{1}$$

$$E_m(t) = \exp\{j[(\omega_s + m\omega_{\mathrm{RF}} + \omega_{35M} + \omega_{40M})(t + \tau_b(t)) + \varphi_m + \varphi_{35M} + \varphi_v(t)]\}, \tag{2}$$

where ω_s and ω_{RF} are the angular frequency of the seed laser and the microwave synthesizer, respectively, φ_n and φ_m are the phase of the nth and mth line of the OFC, respectively, which are locked with each other, ω_{35M} and φ_{35M} are the angular frequency of the 35 MHz AOFS1 drive signal and its initial phase, respectively, and ω_{40M} and $\varphi_v(t)$ are the angular frequency of the 40 MHz AOFS2 drive signal and its phase, respectively. $\tau_a(t)$ and $\tau_b(t)$ are the propagation delay of path "a" and path "b," and we define

$$\varphi_a(t) = (\omega_s + n\omega_{\mathrm{RF}} + \omega_{35M})\tau_a(t), \tag{3}$$

$$\varphi_b(t) = (\omega_s + m\omega_{\mathrm{RF}} + \omega_{35M} + \omega_{40M})\tau_b(t), \tag{4}$$

as the phase fluctuations induced by the two separate optical paths. The amplitude factors are ignored in Eqs. (1) and (2) and in the following equations due to its limited impact on the system.

The mm/THz wave can be generated by heterodyne beating the selected two optical waves at a high-speed PD2. The output of PD2 can be written as

$$I_{mm}(t) = \cos\{[(m-n)\omega_{\mathrm{RF}} + \omega_{40M}]t + \varphi_v(t) + (\varphi_m - \varphi_n) + \varphi_b(t) - \varphi_a(t)\}. \tag{5}$$

From Eq. (5), it can be seen that different frequency signals with a 25 GHz step can be generated by selecting different orders from the OFC. However, the phase of the generated mm/THz wave fluctuates due to the differential phase of the two separated optical fiber paths. Since the phase difference between any two frequencies of the OFC is fixed, in order to achieve a phase-stable mm/THz wave the phase of the AOFS2 drive signal $\varphi_v(t)$ has to be tuned to compensate for the optical-fiber-path-induced phase fluctuation $\varphi_b(t) - \varphi_a(t)$.

The mm-wave phase detection and active phase compensation is realized as follows. The selected two optical waves with a frequency up-shift by AOFS1 and AOFS2 are mixed with the original OFC using a low-frequency PD1 with 100 MHz bandwidth by optical heterodyne beating. Their optical spectra are shown in the inset of Fig. 1. The solid lines indicate the original OFC, while the dotted lines indicate the selected two optical waves from the OFC. Two IF beat signals at 35 and 75 MHz output from PD1 are generated, which can be expressed as

$$I_{\mathrm{IF1}}(t) = \cos[\omega_{35M}t + \varphi_{35M} + \varphi_a(t)], \tag{6}$$

$$I_{\mathrm{IF2}}(t) = \cos[(\omega_{35M} + \omega_{40M})t + \varphi_{35M} + \varphi_v(t) + \varphi_b(t)]. \tag{7}$$

These two IF beat signals are separated by two bandpass filters and then sent to a low-frequency mixer to obtain the differential phase by electrical heterodyne beating. The 40 MHz beat signal from the mixer can be written as

$$V_{\mathrm{IF3}}(t) = \cos[\omega_{40M}t + \varphi_v(t) + \varphi_b(t) - \varphi_a(t)]. \tag{8}$$

Comparing Eq. (8) with Eq. (5), it can be seen that the phase of the IF3 beat signal denotes the optical-fiber-path-induced phase fluctuation of the mm/THz wave. Thus, phase error is obtained by DHPT.

After fourfold dividing $V_{\mathrm{IF3}}(t)$ and comparing it with the 10 MHz rubidium oscillator, the phase error discriminated by a digital phase and frequency detector (PFD) is integrated in the loop filter and then sent to control the frequency of the VCXO and thus its phase $\varphi_v(t)$.

When the PLL is locked by adjusting the frequency of the VCXO, the phase relationship between $V_{\mathrm{IF3}}(t)$ and the rubidium oscillator will satisfy the relation

$$\varphi_v(t) + \varphi_b(t) - \varphi_a(t) = \varphi_{\mathrm{Rb}}, \tag{9}$$

where φ_{Rb} is the initial phase of rubidium oscillator and it is considered as a constant. Substituting Eq. (9) into Eq. (5), the generated mm/THz wave can be expressed as

$$I_{mm}(t) = \cos\{[(m-n)\omega_{\mathrm{RF}} + \omega_{40M}]t + (\varphi_m - \varphi_n) + \varphi_{\mathrm{Rb}}\}. \tag{10}$$

From Eq. (10) it can be seen that the path-induced phase fluctuation of the generated mm/THz wave has been canceled and a highly stable mm/THz wave is obtained.

Figures 2(a)–2(d) show the optical spectra of the selected two optical waves from the OFC with different frequency spacing for generating mm/THz signals. It can be seen that the optical harmonic suppression ratio exceeds 40 dB. Therefore, the effect of residual harmonics can be ignored.

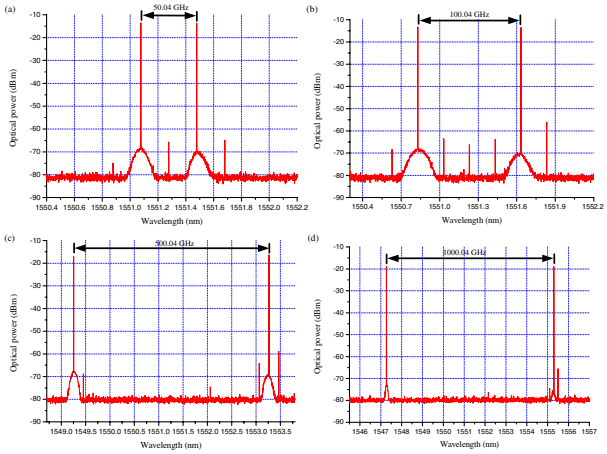

Fig. 2. Optical spectra of the selected optical waves for mm-wave generation. The signal frequencies are (a) 50.04 GHz, (b) 100.04 GHz, (c) 500.04 GHz, and (d) 1000.04 GHz.

In order to prove that the phase error of $V_{\mathrm{IF3}}(t)$ is identical to that of the generated mm/THz wave, the phase noise measurements using a traditional radio frequency (RF) electrical mixer and DHPT scheme are compared at 25 GHz under open and locked cases of the loop. As for the phase detection based on the RF mixer, the generated 25.04 GHz beat signal is mixed with the 25 GHz reference signal from the microwave synthesizer using an electrical RF mixer, as shown in Fig. 3(a). The phase noise of both the IF signals from the RF mixer and $V_{\mathrm{IF3}}(t)$ are analyzed by a phase noise and Allan deviation test set (Symmetricom's 5125A). It can be obviously seen from Fig. 3(b) that the phase characteristics of the two methods are almost consistent, which proves that the single sideband (SSB) residual phase noise of the generated mm/THz wave signal can be denoted by $V_{\mathrm{IF3}}(t)$.

Figure 4 shows the SSB residual phase noise measurements at 50 GHz, 100 GHz, 500 GHz and 1 THz signals under open and locked cases of the loop. The phase noise of these signals is almost unrelated to the frequency of the generated mm/THz wave signals. When the loop is open, the phase fluctuation is induced by temperature variation and mechanical perturbation along the two separated optical fiber paths. The phase noise reaches over 25 dBc/Hz and –30 dBc/Hz at 0.01 and 1 Hz frequency offset from the carrier, respectively. The phase jitter in the frequency range from 0.01 Hz to 1 MHz is about 2.058 rad, which is obtained by integrating the phase noise over the frequency range. When the loop is locked, the phase noise is decreased to under –30 dBc/Hz and –58 dBc/Hz at 0.01-Hz and 1-Hz frequency from the carrier, respectively. The phase jitter in the frequency range from 0.01 Hz to 1 MHz is decreased to about 4.7 mrad. The superimposed waveforms of IF3 in open and locked cases of the loop are also measured in 30 s and 27 min, respectively, by using a digital storage oscilloscope

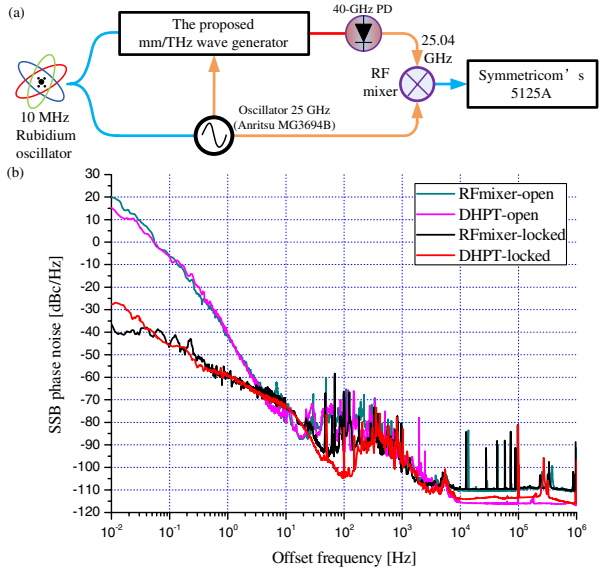

Fig. 3. Comparison of the residual phase noise between the conventional RF mixer and DHPT at 25 GHz. (a) The experimental setup for the RF mixer case, and (b) the measured results.

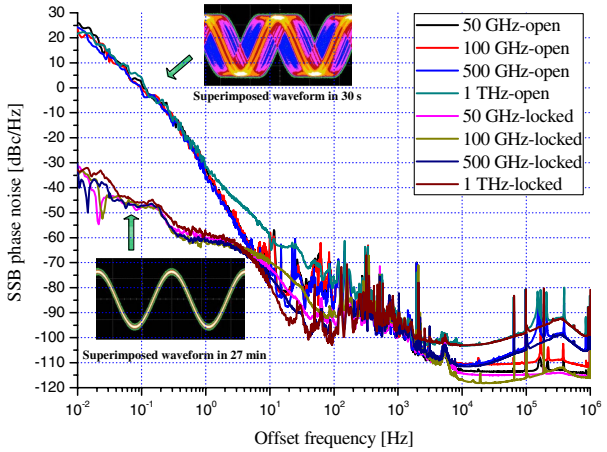

Fig. 4. Residual phase noise of different mm/THz wave signals under open and locked cases of the loop. Insets: superimposed waveforms under open and locked loop cases for IF3.

Table 1. Timing Jitter of the mm/THz Waves

Frequency (GHz)	Open Loop (ps)	Locked Loop (ps)
50.04	6.546	0.015
100.04	3.274	0.007
500.04	0.655	0.0015
1000.04	0.328	0.0007

(Agilent DSO9254A) which is triggered by the rubidium oscillator. As illustrated in the insets of Fig. 4, even over long measurement time, the phase fluctuation is not significantly increased in the locked case of the loop. However, the phase fluctuation for the open loop case is a mess even in the 30 s period, which severely limits practical applications. Moreover, timing jitter can be obtained by dividing the phase jitter by the signal angular frequency, and the timing jitter at different frequencies under the cases of open and locked loops is shown in Table 1.

In summary, a DHPT scheme applied to stabilize the photonic mm/THz wave generation system was experimentally demonstrated in this Letter. Based on the DHPT scheme, the phase information of the generated mm/THz wave was transferred to a 40 MHz IF signal, which overcame the electronic bandwidth limitation of mm/THz wave phase detection. Then, the phase information of the IF signal was used to cancel the phase noise of the mm/THz wave by a phase-locked loop. The highly stable, low-phase-noise mm/THz waves from 25 GHz to 1 THz with a 25 GHz step were successfully generated by this system. The phase noise reached −58 dBc/Hz at 1 Hz frequency offset from the carrier, and the phase jitter in the frequency range from 0.01 Hz to 1 MHz was decreased to 4.7 mrad. Compared with the open loop case, the phase noise performance was improved by a factor of approximately 30 dB at 1 Hz frequency offset, and the phase jitter was reduced from 2.058 rad to 4.7 mrad. We believe the DHPT scheme paves the way for detecting and canceling the phase fluctuation of mm/THz wave signals using low-frequency components and would be applicable to photonic mm/THz wave generation systems through heterodyne beating. By using OFCG with a wider spectral span and higher output power, the system could be extended to higher frequencies.

The authors acknowledge the support of the National Basic Research Program of China (973 Program) (2012CB315602) and the National Natural Science Foundation of China (NSFC) (61225004).

References

1. H. Izadpanah, IEEE Commun. Mag. **39**(9), 140 (2001).
2. Z. Jia, J. Yu, G. Ellinas, and G. K. Chang, J. Lightwave Technol. **25**, 3452 (2007).
3. H. C. Chien, Y. T. Hsueh, A. Chowdhury, J. Yu, and G. K. Chang, J. Lightwave Technol. **28**, 2230 (2010).
4. J. M. Payne, L. R. D'Addario, D. T. Emerson, A. R. Kerr, and B. Shillue, Proc. SPIE **3357**, 143 (1998).
5. J.-F. Cliche and B. Shillue, IEEE Control Syst. Mag. **26**(1), 19 (2006).
6. G. L. Pilbratt, J. R. Riedinger, T. Passvogel, G. Crone, D. Doyle, U. Gageur, A. M. Heras, C. Jewell, L. Mercalfe, S. Ott, and M. Schmidit, Astron. Astrophys. **518**, L1 (2010).
7. M. Tonouchi, Nat. Photonics **1**, 97 (2007).
8. B. Vidal, T. Nagatsuma, N. J. Gomes, and T. E. Darcie, Adv. Opt. Technol. **2012**, 925065 (2012).
9. T. L. Cocker, V. Jelic, M. Gupta, S. J. Molesky, J. A. J. Burgess, G. D. L. Reyes, L. V. Titova, Y. Y. Tsui, M. R. Freeman, and F. A. Hegmann, Nat. Photonics **7**, 620 (2013).
10. M. C. Kemp, P. F. Taday, B. E. Cole, J. A. Cluff, A. J. Fitzgerald, and W. R. Tribe, Proc. SPIE **5070**, 44 (2003).
11. A. Majewski, R. Abreu, and W. Wraback, Proc. SPIE **6549**, 65490B (2007).
12. R. X. Guo, K. Akiyama, H. Minamide, and H. Ito, Appl. Phys. Lett. **90**, 121127 (2007).
13. E. R. Brown, J. E. Bjarnason, A. M. Fedor, and T. M. Korer, Appl. Phys. Lett. **90**, 061909 (2007).
14. A. J. Seeds and K. J. Williams, J. Lightwave Technol. **24**, 4628 (2006).
15. T. Berceli and P. R. Herczfeld, IEEE Trans. Microwave Theory Tech. **58**, 2992 (2010).
16. G. J. Schneider, J. A. Murakowski, C. A. Schuetz, S. Shi, and D. W. Prather, Nat. Photonics **7**, 118 (2013).
17. T. Nagatsuma, A. Hirata, N. Shimizu, H. J. Song, and N. Kukutsu, in *Proceedings of IEEE Conference on Applied Electromagnetics and Communications (ICECOM)* (IEEE, 2007), pp. 1–4.
18. P. Shen, P. A. Davies, W. P. Shillue, L. R. D'Addrio, and J. M. Payne, in *Proceedings of IEEE Conference on Microwave Photonics (MWP)* (IEEE, 2002), pp. 101–104.
19. S. Fukushima, C. F. C. Silva, Y. Muramoto, and A. J. Seeds, J. Lightwave Technol. **21**, 3043 (2003).
20. T. Kuri, T. Nakasyotani, H. Toda, and K. I. Kitayama, IEEE Photon. Technol. Lett. **17**, 1274 (2005).
21. H. J. Song, N. Shimizu, T. Furuta, K. Suizu, H. Ito, and T. Nagatsuma, J. Lightwave Technol. **26**, 2521 (2008).